

Improving performance of piezoelectric energy harvester under electrostatic actuation using cavity

Kourosh Delalat, Mehdi Zamanian* and Behnam Firouzi

Department of Mechanical Engineering, Faculty of Engineering, Kharazmi University, Mofatteh Avenue, P.O. Box 15719-14911, Tehran, Iran

(Received April 27, 2021, Revised June 19, 2021, Accepted October 6, 2021)

Abstract. This study aims to investigate the effect of cavity on electric energy harvesting from cantilever beam vibrations under electrostatic actuation. Electrostatic actuation is created by a layer of radioisotope materials that is placed on the opposite side of the beam emitting electrons. When the beam is charged, the electrostatic force is generated between the beam and the opposite plate and pulls the beam towards itself. After the beam strikes the radioisotope, it is electrically discharged and then released. The piezoelectric layer converts the released microbeam vibration into electricity. The equations of motion coupled with the electrical effects of the piezoelectric layer are extracted using Hamilton's principle and Gauss's law. The equations are discretized by Galerkin method. The exact mode shape of the cantilever beam with the piezoelectric layer is employed as the comparison function. By identifying the relations governing the system, the output voltage and consequently the amount of harvested electrical energy are obtained using various parameters such as thickness and position of the cavity and system electrical resistance. The results indicates that creating cavity has a significant effect on the energy harvesting.

Keywords: cavity; electrostatic; energy harvester; microcantilever; piezoelectric

1. Introduction

Energy harvesting from vibrations has recently received great attention from researchers. These harvesters are also applied in systems that use batteries as a source of energy and it is impossible or expensive to replace the battery (Gurav *et al.* 2004, Murali 2000, Roundy *et al.* 2004, Reddy *et al.* 2016). Energy harvesters fall into three general categories of electromagnetic, electrostatic, and piezoelectric. Although each of these methods can generate an acceptable amount of electrical energy, piezoelectric materials have received more attention than others, the reason for which can be attributed to their ability to directly convert strain energy into electrical energy. Another advantage is their ability to harvest energy at wider frequency ranges (Sodano *et al.* 2004, Abdelkefi *et al.* 2012, Priya 2007) as well as their high output power density. Most of the piezoelectric materials are brittle and are usually not used alone and are mounted on a flexible structure. If voltage is applied to both sides of piezoelectric materials, it causes a strain inside them and, then, they tend to change in length. Thus, if piezoelectric materials are bound to another layer, it causes the substrate layer to bend. Many formulations have been presented for energy harvesting from piezoelectric materials,

*Corresponding author, Ph.D., E-mail: zamanian@khu.ac.ir, zamaniankhu@gmail.com

the most important of which are discussed below.

Different designs of beams have been proposed for maximum energy harvesting (Erturk and Inman 2008, Erturk and Inman 2009, Usharani *et al.* 2017, Zhao *et al.* 2018, Amini *et al.* 2017, Sarker *et al.* 2019, Pan and Dai 2018, Zhang and Zhu 2012, Brufau-Penella and Puig-Vidal 2009, Deepesh *et al.* 2020, Franco and Varoto 2017, Wang *et al.* 2009, Kim *et al.* 2018, Ghodsi *et al.* 2019, Mishra *et al.* 2020, Dutoit *et al.* 2005). Juniour *et al.* (2009) analyzed a plate with a piezoelectric layer under base excitation by finite element method (FEM) and compared the results with experimental results. They used Kirchhoff plate theory to analyze the plate and obtained the equations of motion using Hamilton's method. Chen *et al.* (2012) performed experiments on a circular plate and found that the output energy increased as the frequency decreased. Kim *et al.* (2013) examined three plates with circular, hexagonal, and square geometries coated with piezoelectric layers with a hole in the middle. The piezoelectric area was considered the same in all the three cases. The analysis were performed using FEM by ANSYS software. The output energy of the hexagonal plate was reported to be higher than the others; However, the output energy of the circular plate was very close to it. The output energy increased with a decrease in piezoelectric width and an increase in its length.

Harvesters usually have a standard mass that is adjustable and can be used to approximate the natural frequency of the beam to the excitation frequency of the environment (Abdelkefi *et al.* 2011). Li *et al.* (2010) proposed a beam with L-shaped mass. The lower surface of the L-shaped mass had a curvature that was proportional to the mode shape of the beam, so that the mass had no contact with the beam in the bending state of the beam. The analysis was performed using FEM and ANSYS software. The results were obtained experimentally. There was more mass on the beam in the L-shaped mass model, resulting in more strain as well as more energy. This system had significant output energy at low frequencies.

Guan *et al.* (2013) proposed a structure with an H-shaped mass. This structure induced a large rotational moment of inertia, resulting in a uniform strain distribution in the beam and higher output energy. This structure, with its standard mass and high moment of inertia, occupied little space. In this study, the beam mass and damping were excluded and the analysis was performed using Euler-Bernoulli beam theory. Abdelkafi *et al.* (2011) investigated a cantilever beam with a piezoelectric layer under bending and shear stresses and base excitation and obtained the equations of motion using Hamilton's method. They also developed a simplified model by Galerkin method and extracted transverse displacement, output voltage, angle of twist, and harvested energy. The results indicated the bending-torsional harvesting efficiency increased by 30% compared to the symmetrical sample.

Mehraein *et al.* (2010) examined a conical beam and experimentally concluded that energy harvesting was higher in conical beams than rectangular and trapezoidal beams due to uniform strain distribution. Wang and Chu (2007) proposed a cantilever beam with an air gap between the piezoelectric layers and experimentally indicated the energy harvesting increased with increasing the distance between the piezoelectric layer and neutral axis. Rami *et al.* (2016) experimentally studied a cantilever beam with cavity and actuated its free end by an electric magnet. They found that beams with cavity could harvest more power than beams without cavity. Using vibrations caused by the electrostatic force of radioisotopes has recently received great attention. In these systems, there is usually an electrical voltage between the beam and a fixed surface. With increasing voltage, the beam experiences pull-in phenomenon and strikes the adjacent plate, causing a short circuit. Then, the beam begins to vibrate, and the piezoelectric layer harvests the energy from vibrations. Using radioactive materials is among the existing methods to generate the primary electrostatic force, which is discussed below.

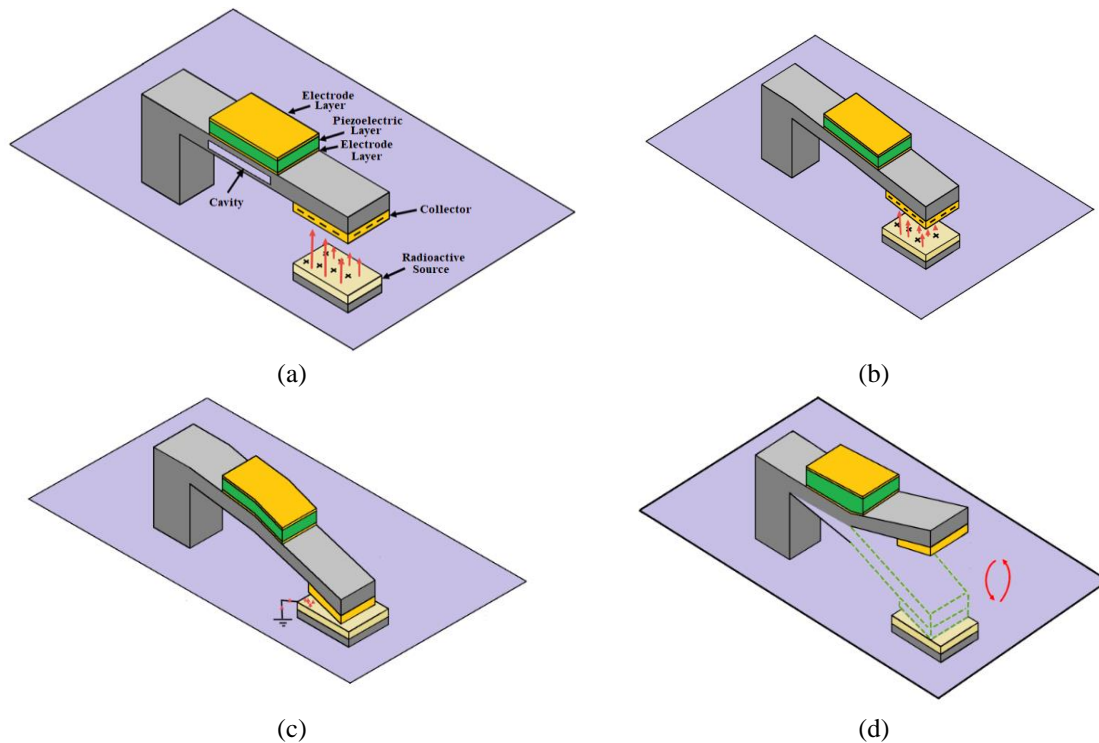


Fig. 1 (a) System configuration, (b) Charging phase, (c) Discharging phase. (d) Vibration of the cantilever

High energy density of radioisotope materials makes them a practical source for generating stable vibrations. Radioactive sources have the energy density of about $1-100 \frac{MJ}{cm^3}$ and half-life of 2-100 years. Although there are many radioisotope sources with high radioactivity, some of which require special and expensive protection. Therefore, choosing an appropriate radioisotope is very important. Dow *et al.* (2011) simplified a piezoelectric harvester operating with a radioactive source into a mass-spring system and solved it by energy method. Zamanian *et al.* (2018) investigated a cantilever microbeam with a piezoelectric layer under radioactive irradiation and extracted the equations of motion nonlinearly considering the electrostatic force and used the mode shape of three-piece beam as the comparison function (Zamanian *et al.* 2018).

Although the electrostatic actuation induced between the beam and opposite radioisotope electrode layer causes the beam to oscillate permanently, which is a convenience source for piezoelectric energy harvester, this question arises how to increase its efficiency. The present study investigates the effect of creating a cavity along the lengths of the beam on the efficiency of energy harvesting in this configuration. In this research, the equations of motion are extracted using Hamilton's principle and Gauss's law and the equations are discretized by Galerkin method. The exact mode shape of the cantilever beam with the piezoelectric layer is used as the comparison function. After finding the relations governing the system, the results are compared with previous results neglecting the effect of cavity to validate the calculations. After indicating the effect of cavity on the performance of piezoelectric energy harvester under electrostatic actuation, the effect of geometric parameters and cavity position on the efficiency of energy harvesting is analyzed.

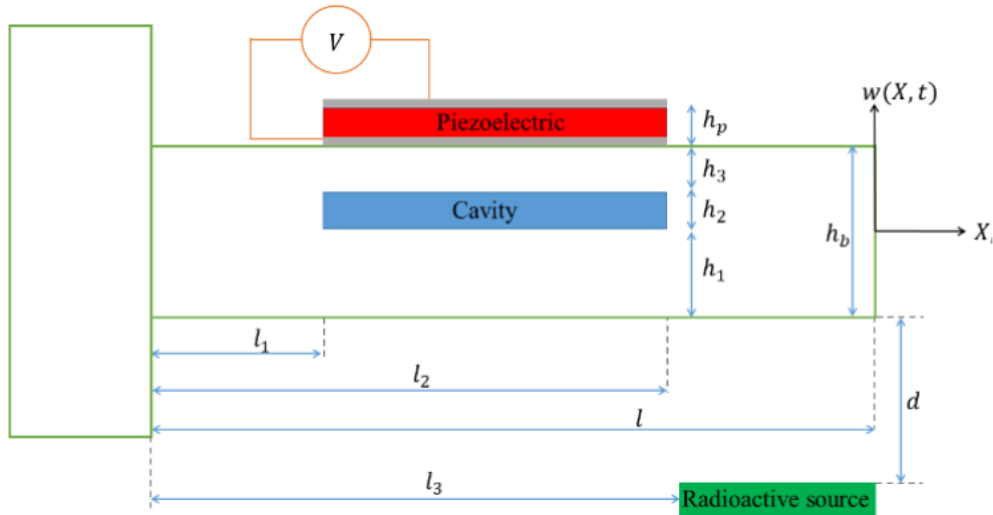


Fig. 2 The cantilever beam with a piezoelectric layer and a cavity along its length.

2. Modeling and formulation

The studied system is a cantilever beam with length l and a rectangular cross-section. A piezoelectric layer with a width equal to the beam width is deposited on the beam, the starting and ending points of which are at distances of l_1 and l_2 from the support, respectively. As shown in Fig. 1, the radioisotope layer is located at a specific distance from the microbeam emitting electrons. There is a time-dependent difference in electrical potential between the microbeam surface and radioisotope layer. This electrical voltage is assumed to be $V_g = kt$ where t represents time and k is a constant. Fig. 1 illustrates the system operation. There is a rectangular cavity right under the piezoelectric layer, the length and width of which are equal to the piezoelectric length and beam width, respectively. The beam length, width, thickness are about a few hundred millimeters, a few tens of millimeters, and a few millimeters, respectively.

A rectangular coordinate system (X, z) is used to extract the equations of motion. Displacement along the z axis is represented by $w(X, t)$ that is a function of time and place. Dot and prime symbols over quantities denote time and place derivatives, respectively. To analyze the beam and extract its equations of motion, it is assumed to have three parts, including before and after the piezoelectric layer and the piezoelectric part. Fig. 2 shows each of these areas. The rectangular cavity is located right under the piezoelectric layer, and the electrodes shown in gray are on either side of the piezoelectric. In this figure, h_b and h_p denote beam and piezoelectric thickness, respectively, h_1 is distance of the lower surface of the cavity from the bottom of the beam, h_2 is cavity height, and h_3 is distance of the top of the cavity from the top of the beam.

Fig. 3(a) shows the beam cross-section before and after of the piezoelectric layer and Fig. 3(b) shows the beam cross-section where the piezoelectric is deposited.

According to Fig. 3, Eq. (1) applies to beam thickness and cavity height.

$$h_1 + h_2 + h_3 = h_b \quad (1)$$

Now, the neutral axis of the beam is obtained in each of these areas. Obviously, in parts where

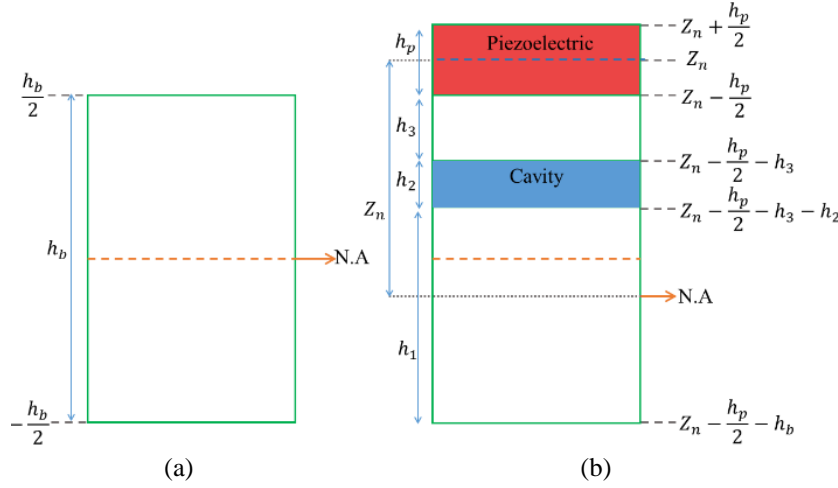


Fig. 3 (a) beam cross-section before and after of the piezoelectric layer, (b) cross-section where the piezoelectric is deposited

there is no piezoelectric layer, the neutral axis passed through the middle axis of the beam cross-section; however, in the part where there is a piezoelectric layer and cavity, the location of the neutral axis should be calculated. The distance of the neutral axis from the middle axis of the piezoelectric is considered to be Z_n . Letting the total force in the cross section of the system equal to zero the following relation is obtained

$$\int_{Z_n - \frac{h_p}{2} - h_b}^{Z_n - \frac{h_p}{2} - h_3 - h_2} E_b z dz + \int_{Z_n - \frac{h_p}{2} - h_3}^{Z_n - \frac{h_p}{2}} E_b z dz + \int_{Z_n - \frac{h_p}{2}}^{Z_n + \frac{h_p}{2}} E_p z dz = 0 \quad (2)$$

where E_b and E_p are elastic modulus of the beam and piezoelectric, respectively. Using Eq. (2), the neutral axis is obtained as bellow

$$Z_n = \frac{E_b(h_2^2 + 2h_2h_3 + h_ph_2 - h_b^2 - h_bh_p)}{2(E_bh_2 - E_bh_b - E_ph_p)} \quad (3)$$

To ensure the correctness of the above equation, h_2 and h_p are assumed to be equal to zero and it is observed that the neutral axis distance is obtained as $Z_n = h_b/2$, which is correct for a simple beam without cavity and piezoelectric. The Hamilton's principle is employed to obtain the equations of motion of the system, for which the potential and kinetic energy of the system is required. First, the potential energy of the system is discussed. The strain potential energy of the system is equal to the total strain energy of the beam and piezoelectric, expressed as follows

$$U_1 = \int_{V_b} \int_0^\varepsilon \sigma_b d\varepsilon dV_b + \int_{V_p} \int_0^\varepsilon \sigma_p d\varepsilon dV_p \quad (4)$$

where σ_b and σ_p represent the stress in the cross section of the beam and piezoelectric layer, respectively, ε denotes strain, and dV is volume element. The total potential energy of the system using the Heaviside function may be written as below

$$\begin{aligned}
U_1 = & \int_0^l \int_{\frac{h_b}{2}}^{\frac{h_b}{2} + \varepsilon} (1 - H_{l_1}) \sigma_b w_b d\varepsilon dz dX + \int_0^l \int_{Z_n - \frac{h_p}{2} - h_2}^{Z_n - \frac{h_p}{2} - h_2 + \varepsilon} (H_{l_1} - H_{l_2}) \sigma_b w_b d\varepsilon dz dX \\
& + \int_0^l \int_{Z_n - \frac{h_p}{2} - h_3}^{Z_n - \frac{h_p}{2}} (H_{l_1} - H_{l_2}) \sigma_b w_b d\varepsilon dz dX + \int_0^l \int_{Z_n - \frac{h_p}{2}}^{Z_n + \frac{h_p}{2}} (H_{l_1} - H_{l_2}) \sigma_p w_b d\varepsilon dz dX \\
& + \int_0^l \int_{\frac{h_b}{2}}^{\frac{h_b}{2} + \varepsilon} H_{l_2} \sigma_b w_b d\varepsilon dz dX
\end{aligned} \tag{5}$$

where w_b is the width of the beam and H_{l_i} is the Heaviside function, and is described as follow

$$H_{l_i} = H(X - l_i) = \begin{cases} 1 & X \geq l_i \\ 0 & X < l_i \end{cases} \quad i = 1, 2 \tag{6}$$

According to Eq. (6), the first term of Eq. (5) indicates the beam potential energy before the piezoelectric layer, the second term represents the beam potential energy at the bottom of the cavity, the third term represents the beam potential energy at the top of the cavity, the fourth term indicates the piezoelectric potential energy, and the fifth term indicates the beam potential energy after the part where the piezoelectric is deposited. Considering the relationships between stress and electrical displacement in piezoelectric and assuming longitudinal stress due to piezoelectric bending as well as considering the direction of the electric field along with the piezoelectric thickness, the beam and piezoelectric stress along with thickness is calculated as bellow

$$\sigma_b = E_b \varepsilon_{11}, \sigma_p = E_p \varepsilon_{11} - e_{31} E_3 \tag{7}$$

where e_{31} is piezoelectric coefficient, and E_3 is the electric field that can be expressed in terms of the voltage across the two ends of the piezoelectric

$$E_3 = -\frac{V}{h_p} \tag{8}$$

The strain is calculated in terms of the beam deflection as follow

$$\varepsilon_{11} = -z \frac{\partial^2 w}{\partial X^2} \tag{9}$$

By replacing Eqs. (9) and (8) into Eq. (7) and replacing Eq. (7) into Eq. (5), the strain potential energy of the system is obtained as follow

$$U_1 = \frac{1}{2} \int_0^l C_\eta(s) \left(\frac{\partial^2 w}{\partial X^2} \right)^2 dX + \int_0^l C_\gamma V \frac{\partial^2 w}{\partial X^2} dX \tag{10}$$

where V is the potential difference in the piezoelectric layer and C_η and C_γ can be calculated as follows

$$\begin{aligned}
C_\eta = & (1 - H_{l_1}) E_b I_{1b} + (H_{l_1} - H_{l_2}) E_b I_{2b} + (H_{l_1} - H_{l_2}) E_b I_{3b} \\
& + (H_{l_1} - H_{l_2}) E_p I_p + H_{l_2} E_b I_{1b}
\end{aligned} \tag{11}$$

$$C_\gamma = (H_{l_1} - H_{l_2}) \frac{e_{31}A_p}{h_p} \tag{12}$$

where the coefficients presented in Eqs. (11) and (12) are defined as follows

$$\begin{aligned} I_{1b} &= w_b \frac{h_b^3}{12} \\ I_{2b} &= \frac{w_b}{3} (h_b^3 - h_3^3 - h_2^3 - 3Z_n^2 h_3 - 3Z_n^2 h_2 - 3Z_n h_3^2 + 3Z_n h_2^2 - \frac{3}{4} h_p^2 h_3 - \frac{3}{4} h_p^2 h_2 \\ &\quad - \frac{3}{2} h_p h_3^2 - \frac{3}{2} h_p h_2^2 - 3h_3^2 h_2 - 3h_2^2 h_3 + 3Z_n^2 h_b - 3Z_n h_b^2 + \frac{3}{4} h_p^2 h_b + \frac{3}{2} h_p h_b^2 \\ &\quad + 3Z_n h_p h_3 - 3Z_n h_p h_b - 3h_p h_3 h_2 + 3Z_n h_p h_2 + 6Z_n h_3 h_2) \\ I_{3b} &= \frac{w_b}{3} (3Z_n^2 h_3 - 3Z_n h_p h_3 - 3Z_n h_3^2 + \frac{3}{4} h_p^2 h_3 + \frac{3}{2} h_p h_3^2 + h_3^2) \\ I_p &= \frac{w_b}{3} (3Z_n^2 h_p + \frac{1}{4} h_p^3) \\ A_p &= w_b Z_n h_p \end{aligned} \tag{13}$$

Now, the electrostatic potential energy generated by the radioisotope under the beam is calculated. This radioisotope modeling has been performed by Dow *et al.* (2011). Considering the differential equations governing the radioisotope, the electrostatic potential energy is calculated as follows (Firouzi and Zamanian 2019)

$$U_2 = -\frac{1}{2} \int_0^l H_{l_3} \epsilon_0 w_b \frac{V_g^2}{d+w} dX \tag{14}$$

where ϵ_0 is vacuum electric permittivity, V_g is time-dependent voltage between the beam and radioisotope, and d is distance between the beam and radioisotope. The kinetic energy is calculated may be obtained as bellow

$$T = \frac{1}{2} \int_0^l m(X) \left(\frac{\partial w}{\partial t}\right)^2 dX \tag{15}$$

where $m(x)$ is mass per unit length which can be expressed as

$$m(X) = w_b (\rho_b h_b + (H_{l_1} - H_{l_2}) (\rho_p h_p - \rho_b h_2)) \tag{16}$$

Finally, considering damping as an external force, the external work applied to the system due to damping is calculated as follow

$$\delta W_F = \int_0^l \left(-c \frac{\partial w}{\partial t} \delta w\right) dX \tag{17}$$

where c is the coefficient of external viscous damping. Having potential energy, kinetic energy, and external work of the system, the equations of motion were obtained using Hamilton's principle.

$$\delta \int (T - U_1 - U_2 + W_F) dt = 0 \tag{18}$$

By substituting Eqs. (17), (15), (14), (10) into Eq. (18), equation of motion is obtained as follow

$$\frac{\partial}{\partial t} \left(m(x) \frac{\partial w}{\partial t}\right) + \frac{\partial^2}{\partial X^2} \left(C_\eta \frac{\partial^2 w}{\partial X^2}\right) + \frac{\partial}{\partial X^2} (C_\gamma V) + C_\lambda V_g^2 \frac{1}{(d+w)^2} + c \frac{\partial w}{\partial t} = 0 \tag{19}$$

where C_λ is

$$C_\lambda = \frac{1}{2} \varepsilon_0 w_b H_{l_3} \quad (20)$$

Boundary conditions can be expressed as

$$\begin{aligned} w|_{x=0} = 0, \quad \frac{\partial w}{\partial X}|_{x=0} &= 0 \\ \frac{\partial^2 w}{\partial X^2}|_{x=l} = 0, \quad \frac{\partial^3 w}{\partial X^3}|_{x=l} &= 0 \end{aligned} \quad (21)$$

For convenience, the following set of non-dimensional parameters are introduced

$$v = -\frac{w}{h_b}, \quad x = \frac{X}{l}, \quad \tau = \frac{t}{T}, \quad T = \sqrt{\frac{\rho_b w_b h_b l^4}{E_b I_{1b}}} \quad (22)$$

Considering the non-dimensional parameters, the equation of motion and governing boundary conditions can be expressed as Eqs. (23) and (24).

$$m(x) \frac{\partial^2 v}{\partial \tau^2} + C \frac{\partial v}{\partial \tau} + \frac{\partial^2}{\partial x^2} \left(H(x) \frac{\partial^2 v}{\partial x^2} \right) - \alpha_1 V \frac{d^2}{dx^2} \left(\frac{H_{l_1}}{l} - \frac{H_{l_2}}{l} \right) - \gamma V_g^2 \frac{1}{\left(\frac{d}{h_b} - v \right)^2} = 0 \quad (23)$$

$$v|_{x=0} = 0, \quad \frac{\partial v}{\partial x}|_{x=0} = 0, \quad \frac{\partial^2 v}{\partial x^2}|_{x=1} = 0, \quad \frac{\partial^3 v}{\partial x^3}|_{x=1} = 0 \quad (24)$$

Where

$$\begin{aligned} m(x) &= 1 + (H_{\frac{l_1}{l}} - H_{\frac{l_2}{l}}) \frac{(\rho_p h_p - \rho_b h_2)}{\rho_b h_b}, \\ C &= \sqrt{\frac{l^4}{\rho_b h_b w_b E_b I_{1b}}} c, \\ \alpha_1 &= \frac{e_{31} A_p l^2}{h_p E_b I_b h_b}, \quad \gamma = \frac{\varepsilon_0 w_b H_{l_3}}{2 h_b^2}, \end{aligned} \quad (25)$$

$$H(x) = \left(1 - H_{\frac{l_1}{l}}\right) + \left(H_{\frac{l_1}{l}} - H_{\frac{l_2}{l}}\right) \frac{I_{2b}}{I_{1b}} + \left(H_{\frac{l_1}{l}} - H_{\frac{l_2}{l}}\right) \frac{I_{3b}}{I_{1b}} + \left(H_{\frac{l_1}{l}} - H_{\frac{l_2}{l}}\right) \frac{E_p I_p}{E_b I_b} + H_{\frac{l_2}{l}}$$

Gauss's law, also known as Gauss's flux theorem, is a law in physics that states the relationship between electric charge (Q) and electric displacement (D). The integral form of this law is as Eq. (26).

$$Q = \int_A D \cdot ndA \quad (26)$$

where A is a closed surface and Gauss's law relates the electric displacement of this surface to the electric charge enclosed within it. Using the definition of electric current, it can be written

$$\frac{dQ}{dt} = I \Rightarrow \frac{d}{dt} \int_A D \cdot ndA = I \quad (27)$$

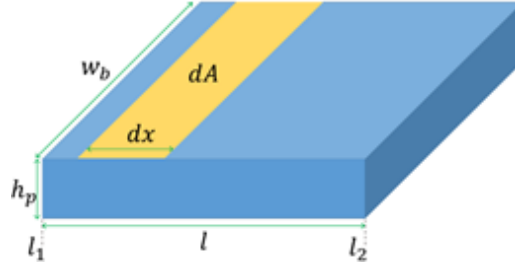


Fig. 4 Surface element of the piezoelectric layer

Also, using Ohm's law, where $\frac{V}{R} = I$, it can be written

$$\frac{d}{dt} \int_A D \cdot n dA - \frac{V}{R} = 0 \tag{28}$$

Considering piezoelectric as a surface enclosed in Gauss's law and using piezoelectric structural relations, the output voltage equation of the system is obtained. Considering the equation of piezoelectric structure, the following equation is obtained for electric displacement along the z axis (Zamanian *et al.* 2018)

$$D_3 = e_{31} \varepsilon_{11} + \epsilon_{33} E_3 \tag{29}$$

where e_{31} is piezoelectric coefficient, ε_{11} is longitudinal strain or the same as σ_p , ϵ_{33} is electrical permittivity factor (dielectric constant), and E_3 is electric field along the z direction. By replacing Eq. (29) into Eq. (28), it can be written

$$\frac{d}{dt} \int_A e_{31} \varepsilon_{11} dA + \frac{d}{dt} \int_A \epsilon_{33} E_3 dA - \frac{V}{R} = 0 \tag{30}$$

Considering the surface element in Fig. 4 for the second term of Eq. (30) and including Eq. (9), the following equation is obtained.

$$\frac{d}{dt} \int_A -e_{31} z w'' dA + \frac{d}{dt} \int_{l_1}^{l_2} \epsilon_{33} E_3 w_b dX - \frac{V}{R} = 0 \tag{31}$$

Using divergence theorem, the first term of the above equation can be rewritten as follows, in which the integration is performed on the volume of the piezoelectric layer.

$$\int_A -e_{31} z w'' dA = \int_{V_p} \nabla \cdot (-e_{31} z w'') dV_p = \int_{V_p} \frac{\partial}{\partial z} (-e_{31} z w'') dV_p \tag{32}$$

By substituting Eq. (8) into Eq. (30) and using Eq. (32), the following relation will be obtained

$$\frac{d}{dt} \int_{V_p} -e_{31} w'' dV_p + \frac{d}{dt} \int_{l_1}^{l_2} -\epsilon_{33} \frac{V(t)}{h_p} w_b dX - \frac{V(t)}{R} = 0 \tag{33}$$

According to Fig. 4, the volume element is considered as $dV_p = h_p w_b dX$. Then, by calculating the integrals, the relationship between output voltage and dynamic deflection is obtained as follows

$$e_{31}h_p w_b \frac{\partial^2 w}{\partial X \partial t} \Big|_{l_1}^{l_2} + \frac{\epsilon_{33} w_b (l_2 - l_1)}{h_p} \frac{dV(t)}{dt} + \frac{V(t)}{R} = 0 \quad (34)$$

By applying the dimensionless quantities in Eq. (22), it can be written

$$-\frac{e_{31}h_p w_b h_b}{lT} \frac{\partial^2 v}{\partial x \partial \tau} \Big|_{\frac{l_1}{l}}^{\frac{l_2}{l}} + \frac{\epsilon_{33} w_b (l_2 - l_1)}{h_p T} \frac{dV(\tau)}{d\tau} + \frac{V(\tau)}{R} = 0 \quad (35)$$

Finally, Eq. (35) is the electrical relationship governing the system under consideration, which will be used later.

3. Solving equations of motion

In the previous section a set of coupled equations between the dynamic deflection and output electric voltage were extracted. In this section, these relations are solved, and so the dynamic deflection and output electric voltage are calculated.

Galerkin method is used to solve Eq. (23). Therefore the function $v(x, \tau)$ is written as follow

$$v(x, \tau) = \sum_1^N \phi_i(x) p_i(\tau) \quad (36)$$

where $\phi_i(x)$, the spatial part of the response, is a function that satisfies the boundary conditions of the problem. The exact mode shape of the system described at the appendix are used as the comparison functions. $p_i(\tau)$ is time coordinate of the response, obtained by Galerkin method. Taylor expansion was also employed to simplify the electrostatic force as follow

$$\frac{1}{\left(\frac{d}{h_b} - v\right)^2} = \frac{h_b^2}{d^2} + \frac{2h_b^3}{d^3} v + \frac{3h_b^4}{d^4} v^2 + \frac{4h_b^5}{d^5} v^3 \quad (37)$$

By substituting Eqs. (36) and (37) into differential Eq. (23) and multiplying the resulting equation by $\phi_j(x)$, such that $j = 1..N$, and integrating it at the interval $x = 0..1$, a set of ordinary coupled equations are obtained.

$$\begin{aligned} eq_j = & \sum_1^N \left(\frac{d^2 p_i(\tau)}{d\tau^2} \int_0^1 m(x) \phi_j(x) \phi_i(x) dx + C \frac{dp_i(\tau)}{d\tau} \int_0^1 \phi_j(x) \phi_i(x) dx \right. \\ & + p_i(\tau) \int_0^1 \phi_j(x) \frac{d^2}{dx^2} \left(H(x) \frac{d^2 \phi_i(x)}{dx^2} \right) dx \Big) - \alpha_1 V(\tau) \int_0^1 \phi_j \frac{d^2}{dx^2} \left(H_{\frac{l_1}{l}} - H_{\frac{l_2}{l}} \right) dx \\ & - V_g^2(\tau) \left(\alpha_2 \int_0^1 H_{\frac{l_3}{l}} \phi_j(x) dx + \alpha_3 p_i(\tau) \int_0^1 H_{\frac{l_3}{l}} \phi_j(x) \phi_i(x) dx \right. \\ & \left. + \alpha_4 p_i^2(\tau) \int_0^1 H_{\frac{l_3}{l}} \phi_j(x) \phi_i^2(x) dx + \alpha_5 p_i^3(\tau) \int_0^1 H_{\frac{l_3}{l}} \phi_j(x) \phi_i^3(x) dx \right) = 0 \end{aligned} \quad (38)$$

where α_2 , α_3 , α_4 and α_5 are stated as

$$\alpha_2 = \frac{\epsilon_0 w_b}{2d^2}, \alpha_3 = \frac{\epsilon_0 w_b h_b}{d^3}, \alpha_4 = \frac{3\epsilon_0 w_b h_b^2}{2d^4}, \alpha_5 = \frac{2\epsilon_0 w_b h_b^3}{d^5} \quad (39)$$

The third term of Eq. (38) can be simplified by integration by parts as follows

$$\begin{aligned} \int_0^l \phi_j(x) \frac{d^2}{dx^2} \left(H(x) \frac{d^2 \phi_i(x)}{dx^2} \right) dx &= \phi_j(x) \frac{d}{dx} \left(H(x) \frac{d^2 \phi_i(x)}{dx^2} \right) \Big|_0^l - \\ \int_0^l \frac{d\phi_j(x)}{dx} \frac{d}{dx} \left(H(x) \frac{d^2 \phi_i(x)}{dx^2} \right) dx &= \phi_j(x) \frac{d}{dx} \left(H(x) \frac{d^2 \phi_i(x)}{dx^2} \right) \Big|_0^l - \frac{d\phi_j(x)}{dx} H(x) \frac{d^2 \phi_i(x)}{dx^2} \Big|_0^l + \\ &\int_0^l \frac{d^2 \phi_j(x)}{dx^2} H(x) \frac{d^2 \phi_i(x)}{dx^2} dx \end{aligned} \quad (40)$$

By applying the boundary conditions of Eq. (24), the first two terms of Eq. (40) became equal to zero and it may be rewritten as follows

$$\int_0^l \phi_j(x) \frac{d^2}{dx^2} \left(H(x) \frac{d^2 \phi_i(x)}{dx^2} \right) dx = \int_0^l \frac{d^2 \phi_j(x)}{dx^2} H(x) \frac{d^2 \phi_i(x)}{dx^2} dx \quad (41)$$

Also, Eq. (42) is used to simplify the fourth term of Eq. (38) as follows

$$\int f(x) \frac{d^2}{dx^2} (\text{Heaviside}(x - a)) dx = -\frac{df}{dx} \quad (42)$$

Using Eq. (42), the fourth term of Eq. (38) can be stated as follows

$$\alpha_1 V(\tau) \int_0^1 \phi_j \frac{d^2}{dx^2} \left(H_{\frac{l_1}{l}} - H_{\frac{l_2}{l}} \right) dx = -\alpha_1 V(\tau) \left(\frac{d\phi_j(x)}{dx} \Big|_{\frac{l_1}{l}} - \frac{d\phi_j(x)}{dx} \Big|_{\frac{l_2}{l}} \right) \quad (43)$$

By incorporating Eqs. (41) and (38), Eq. (40) is obtained as follows

$$\begin{aligned} eq_j &= \sum_1^N \left(\frac{d^2 p_i(\tau)}{d\tau^2} \int_0^1 m(x) \phi_j(x) \phi_i(x) dx + C \frac{dp_i(\tau)}{d\tau} \int_0^1 \phi_j(x) \phi_i(x) dx \right. \\ &+ \int_0^l \frac{d^2 \phi_j(x)}{dx^2} H(x) \frac{d^2 \phi_i(x)}{dx^2} dx \left. \right) + \alpha_1 V(\tau) \left(\frac{d\phi_j(x)}{dx} \Big|_{\frac{l_1}{l}} - \frac{d\phi_j(x)}{dx} \Big|_{\frac{l_2}{l}} \right) \\ &- V_g^2(\tau) \left(\alpha_2 \int_0^1 H_{\frac{l_2}{l}} \phi_j(x) dx + \alpha_3 p_i(\tau) \int_0^1 H_{\frac{l_2}{l}} \phi_j(x) \phi_i(x) dx \right. \\ &\left. + \alpha_4 p_i^2(\tau) \int_0^1 H_{\frac{l_2}{l}} \phi_j(x) \phi_i^2(x) dx + \alpha_5 p_i^3(\tau) \int_0^1 H_{\frac{l_2}{l}} \phi_j(x) \phi_i^3(x) dx \right) = 0 \end{aligned} \quad (44)$$

By substituting Eq. (36) into Eq. (35) and multiplying the outcome by ϕ_i , and integrating from $x=0$ to $x=1$, one obtains

$$\sum_{i=1}^N \left(-\frac{\epsilon_{31} h_p w_b h_b}{lT} \frac{d\phi_i}{dx} \Big|_{\frac{l_1}{l}}^{\frac{l_2}{l}} \frac{dp_i}{d\tau} \right) + \frac{\epsilon_{33} w_b (l_2 - l_1)}{h_p T} \frac{dV(\tau)}{d\tau} + \frac{V(\tau)}{R} = 0 \quad (45)$$

Eqs. (45) and (44) are numerically solved using Maple software simultaneously. These equations are solved by Runge-Kutta numerical method. The dynamic deflection of the system and output voltage of the piezoelectric layer are obtained based on time variations. The following equation is used to calculate the system output power

Table 1 System dimensions

l	E_b	E_p	h_b	h_p	ρ_b	ρ_p	w_b	e_{31}	ϵ_{33}	l_1	l_2
276	71	47.62	6	0.5	2700	7500	25	-16.6	2.55	40	116
mm	Gpa	Gpa	mm	mm	kg/m ³	kg/m ³	mm	C/m ²	F/m	mm	mm

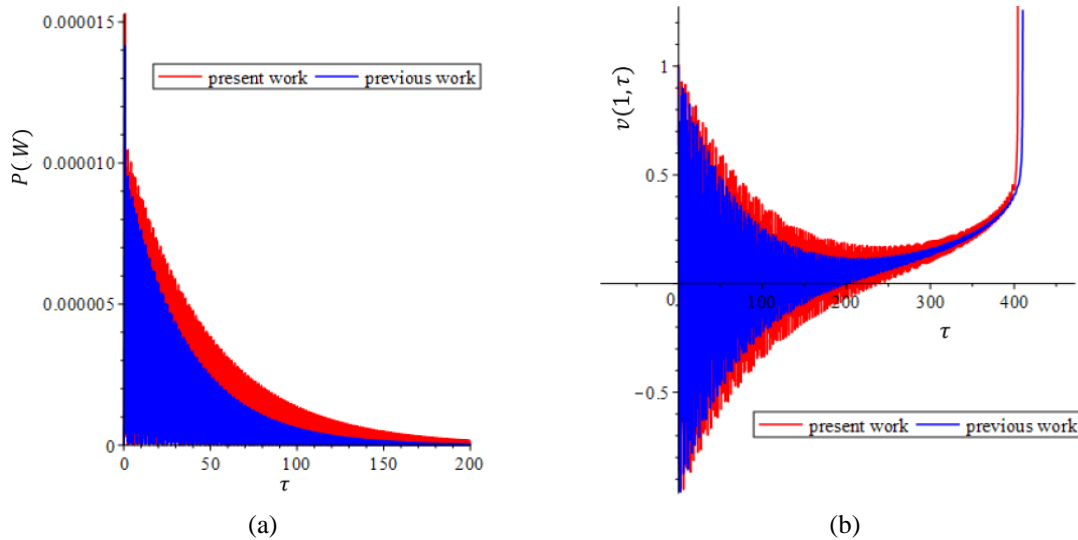


Fig. 5 Comparing (a) output power, and (b) time history of the present work with the outcomes of the previous work (Zamanian *et al.* 2018)

$$P = \frac{V^2}{R} \quad (46)$$

4. Results and discussion

The results presented in this section are divided into three parts. The first part deals with the validation of the results by a comparison with the previous work assuming the absence of the cavity. The second part indicates that harvested energy increases when the configuration includes a cavity. The third part presents a more detailed study of the effects of the cavity position and geometry on the energy efficiency and energy harvesting. The system dimensions are presented in Table 1.

Considering the absence of the cavity and using the same characteristics as the previous work (Zamanian *et al.* 2018), the results are compared together. As shown in Fig. 5(a) and 5(b), there is a good agreement between the present work and the previous work (Zamanian *et al.* 2018). It indicates the accuracy of the calculations of the present work. In Fig. 5 the initial condition of the beam is assumed in discharging position i.e., the beam is initially attached to the electrode layer. As can be seen in this diagram, by starting the vibration of the system the electrostatic force causes that systems oscillates around a new position in each cycle. It demonstrates that the new position in each cycle increases by increasing time, and the amplitude of the vibration decreases. By more increase of the time the electrostatic force overcomes the beam stiffness, and the system will be unstable. In means that the beam suddenly moves toward the electrode layer, and pull-in occurs. In other words

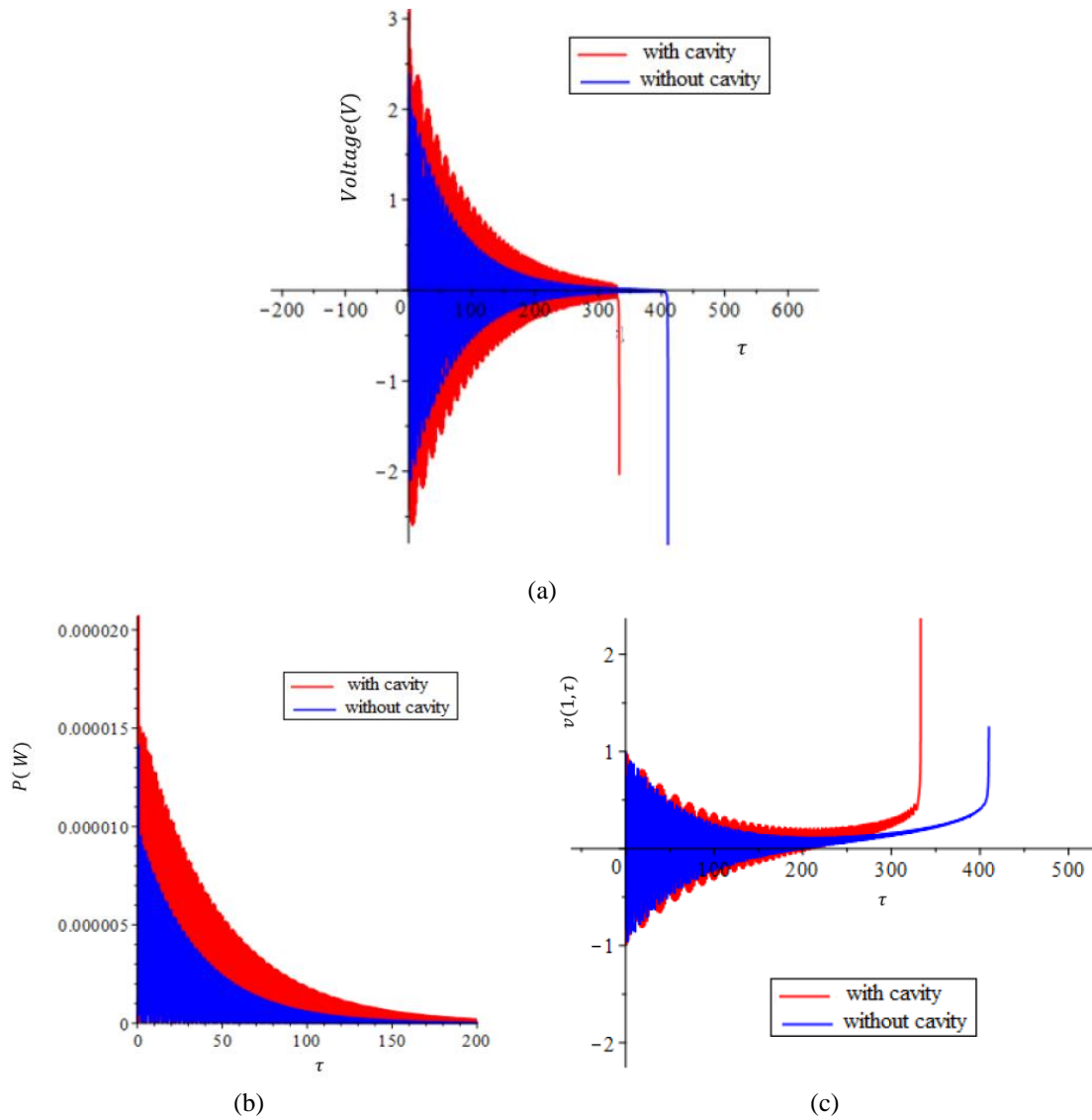


Fig. 6 Comparing (a) voltage, (b) output power, and (c) time history of the system oscillations with and without cavity

due to the presence of the electrostatic force, the vibration equilibrium position moved away from straight position, and each time the beam is vibrated around a new position that is far from straight position and is closer to the radioisotope electrode. As shown in figures, pull-in phenomenon occurs when the slope of the curve approaches toward the infinity.

Figs. 6(a) and 6(c) compare the systems in two cases. The first case assumed the system with cavity and the second case considers it without cavity. The physical characteristics of the two systems were the same and the only difference was the presence of a cavity with the height of about two thirds of the beam thickness and close to the upper surface of the beam. It shows that the voltage and power harvesting significantly increases in the presence of the cavity. It must be noted that the

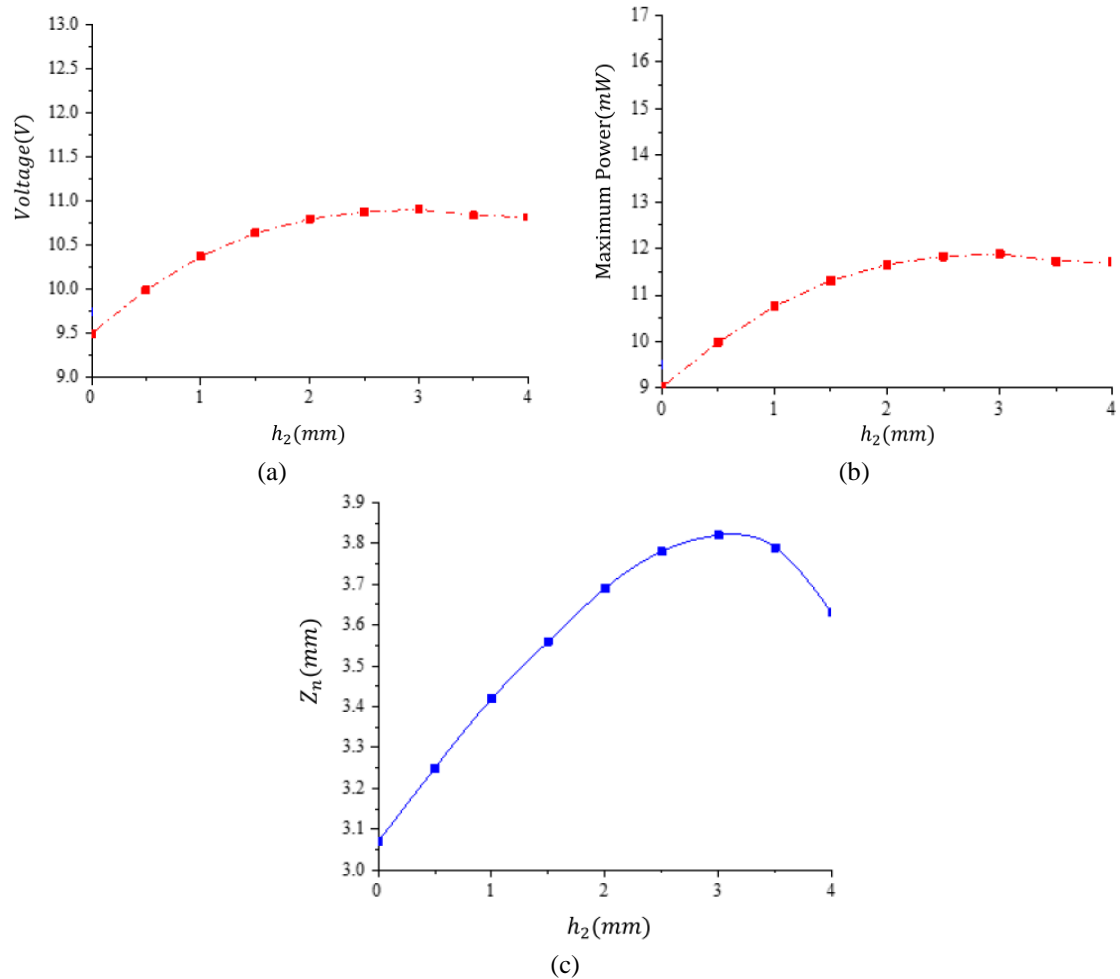


Fig. 7 Variation of (a) maximum voltage, (b) maximum power and (c) neutral axis, for different values of cavity thickness (h_2)

earlier occurrence of the pull-in phenomenon in the beam with cavity is due to the lower equivalent stiffness of the beam. In the present work, the maximum voltage (V_{\max}) is 3.13, which has been increased by 19.4% compared to the system without cavity, in which the maximum voltage was 2.62. Also, the output power (P_{\max}) is obtained as $20.23 \mu\text{W}$ in the present work, which has been increased by 42.1% compared to the system without cavity, in which the output power was $14.23 \mu\text{W}$.

In this section, diagrams of maximum voltage and output power are presented in terms of beam geometry changes. Figs. 7(a) and 7(b) illustrate the variations of maximum output voltage and electrical power by increasing the cavity thickness. It shows that the output voltage and electrical power increases by increasing the cavity thickness, such that they reaches the maximum level, and then their values decreases. The maximum value of these parameters occurs when the thickness of cavity is approximately equal to 3 mm. The reason for such changes can be attributed to the changes of the position of bending neutral axis shown in Fig. 7(c). As can be observed, the amount of z_n

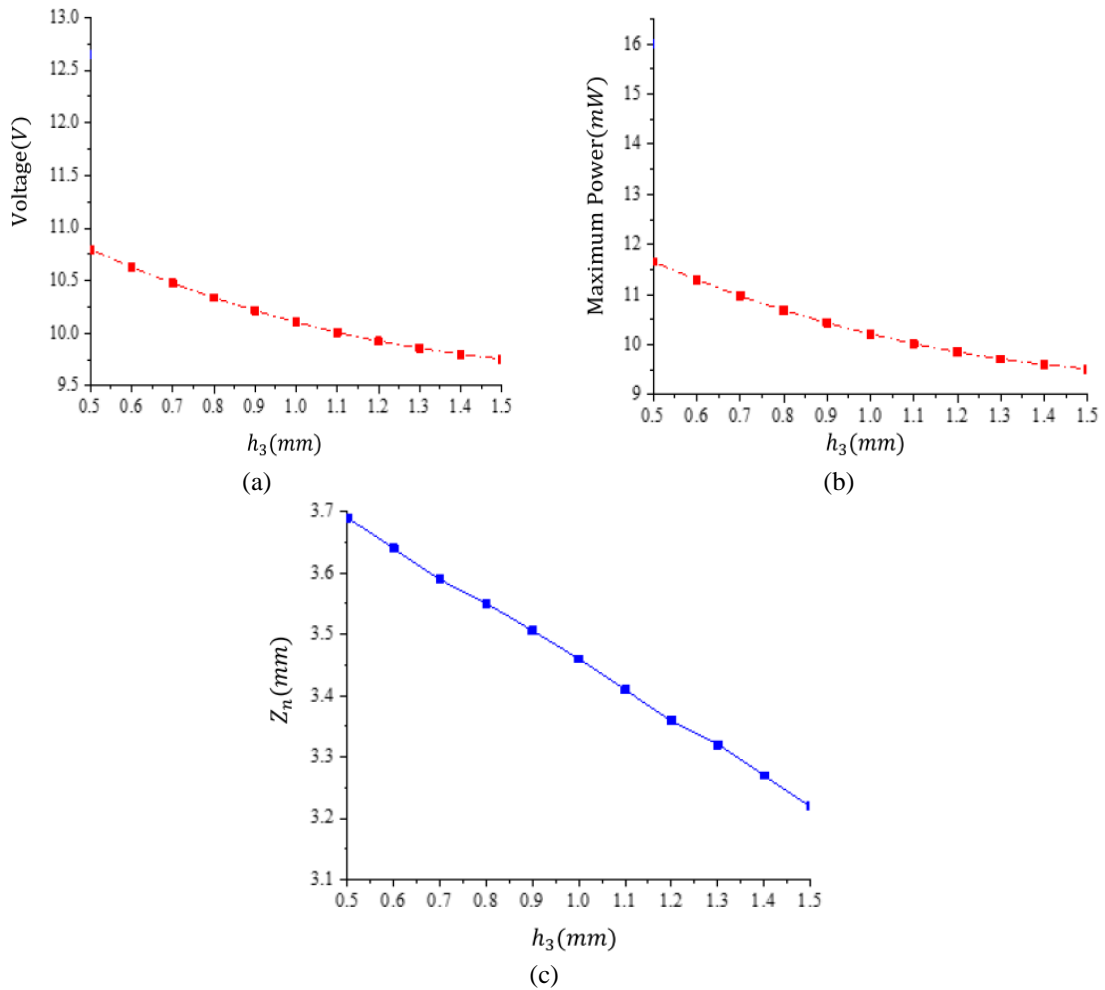


Fig. 8 Variation of (a) maximum voltage, (b) maximum power and (c) neutral axis, for different values of cavity position (h_3)

has its maximum value when the cavity thickness is approximately equal to 3 mm. It means that in this condition the piezoelectric layer is at the greatest distance from the neutral surface. In the beams under bending, the axial stress increases by moving away from the neutral surface. Therefore, the stress and strain of the piezoelectric layer will be maximum in this case. According to Eq. (29), increasing the strain of the piezoelectric material causes an increase of the electric displacement and consequently the electrical output voltage.

Figs. 8(a) and 8(b) indicate the effect of cavity distance from the upper surface of the beam (h_3) on the maximum output voltage and electrical power. This figure shows that the maximum output voltage and electrical power decreases when the cavity moved away from the top of the beam and approached the middle of the beam i.e., when the amount of h_3 increases. The reason of this behavior is that according to Fig. 8(c), the amount of z_n decreases by increasing the amount of h_3 . It means that neutral axis moved upwards by increasing the distance of the cavity from the top of the beam. In other words, the neutral axis will be closer to the piezoelectric layer. The result of

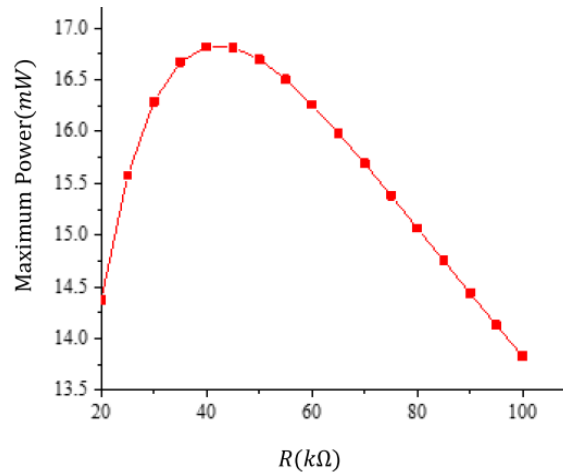


Fig. 9 Variations of the electrical power with respect to the variations of electrical resistance

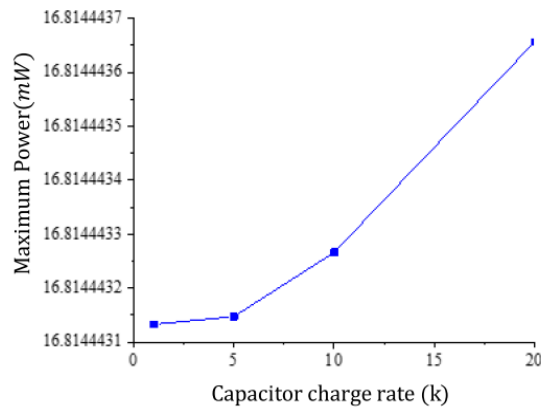


Fig. 10 Variations of the maximum output electrical power with respect to the rate of capacitor charging (k)

these changes, for the same reason as stated in the previous paragraph, led to a reduction in maximum voltage and output electrical power. Considering both geometric changes of the cavity, i.e., increasing its thickness as well as its distance from the upper surface of the beam, it is found that a cavity with thickness equal to 3 mm and distance from the upper surface of the beam equal to 0.5 mm could provide the highest rate of power harvesting.

It must be noted that a parameter that is important for the design of a harvester energy is its life span. Absolutely creating a cavity along the lengths of the beam decreases the life span of system. However the relation between the size of the cavity and life span of the system has not been studied in this paper, and it may be studied in future works. Certainly there is an optimum dimension for the cavity to obtain a good performance and also a long span life.

Fig. 9 shows the effect of electrical resistance on the maximum output electrical power of the system. It demonstrates that the maximum electrical output power increases and then decreases by an increase of electrical resistance of the piezoelectric layer. Fig. 9 illustrates that the maximum power of 16.821 (mW) is obtained when the electrical resistance is approximately 40 $k\Omega$.

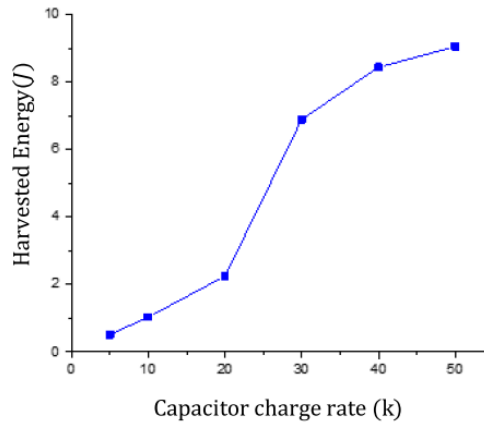


Fig. 11 Variations of the output electrical power with respect to the rate of capacitor charging (k) during 2000 sec

Fig. 10 shows the effect of voltage charge rate by the radioactive material on the maximum harvested electrical power. As mentioned earlier, the charge of a capacitor consisting of a beam and radioisotope is almost linear. Therefore it is assumed that the voltage difference between the beam and opposite electrode layer is $v_g=kt$. Fig. 10 states that the amount of k has a little effect on the maximum output power, and its values remains constant approximately equal to 16.81. However, the important point is that the pull-in phenomenon occurs faster when k is larger, so more energy could be harvested over a specific period of time. For example, the pull-in phenomena occurs 42 times for a system with $V_g = 50$ t during 2000 second. In this period of time the harvested energy will be approximately equal to 9J. When $V_g = 5$ t the pull-in phenomena happens only once, and therefore the total harvested energy will 520 mJ. It means that according Fig. 11 more energy could be harvested for a system with higher value of k in the same period of time. It should be noted that if the pull-in period is greatly reduced, the beam would not have a chance to vibrate and the total harvested energy would be decreased.

As mentioned earlier, the maximum power is not the only criterion for energy harvesting, but the number of times the system experiences pull-in phenomenon is also important. Although this issue can be changed by radioisotopes, these materials also have some limitations and cannot create any charge rate. Therefore, changing the system dimensions is the best solution. It is necessary to investigate the effect of the cavity position and thickness on the period required for pull-in phenomenon.

Fig. 12 indicate the system time history diagrams considering changes in the cavity geometry. Comparing Fig. 12(a) with 12(b) reveals that the pull-in phenomenon occurs earlier by increasing the cavity thickness (h_2) from 2 mm to 3 mm. Also, comparing Fig. 12(a) with 12(c) indicates that the pull-in phenomenon occurs later by increasing the cavity distance from the upper surface of the beam, i.e., changing h_3 from 0.5 mm to 1 mm.

5. Conclusions

In this work the energy harvesting by a piezoelectric layer from the oscillations of a cavitad

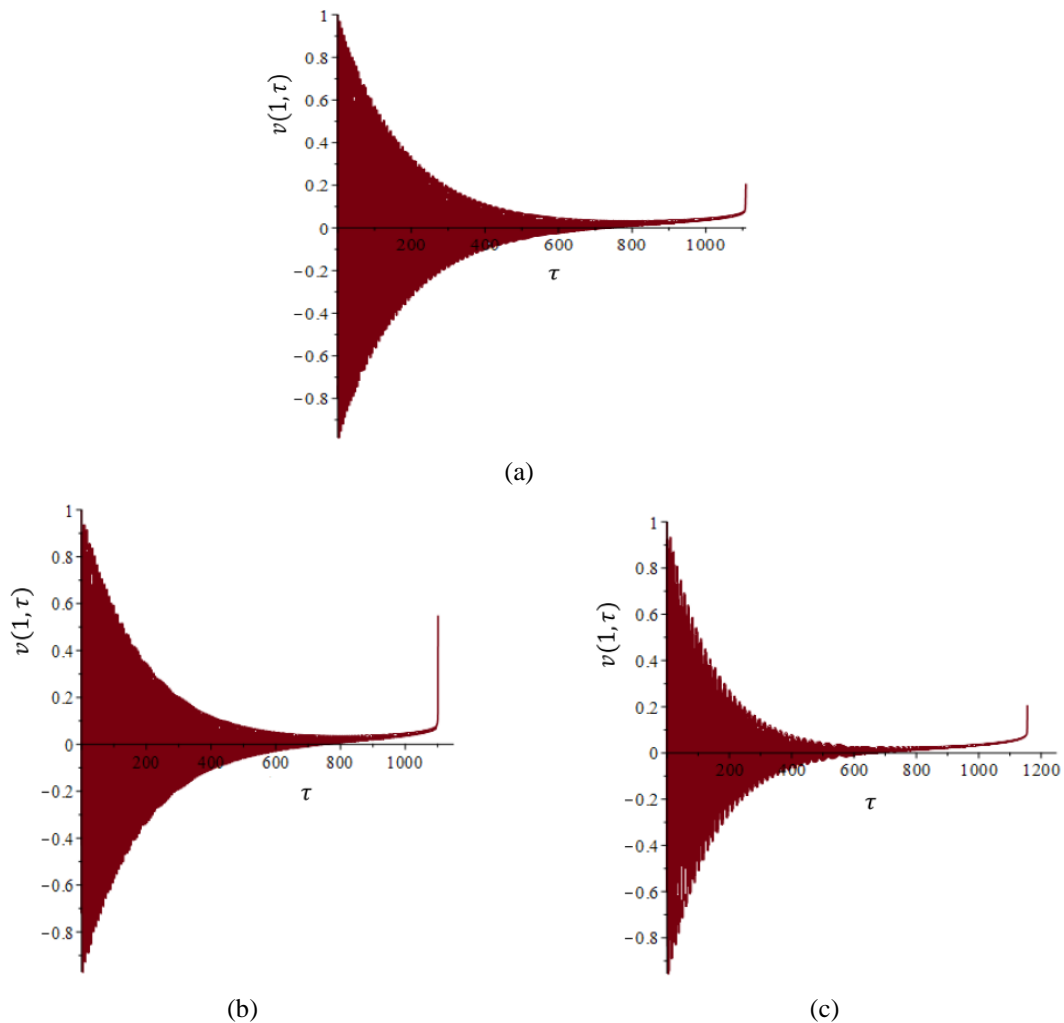


Fig. 12 Time history of the system for (a) $h_2=2$ mm (b) $V_g=10$ t, $h_3=0.5$ mm, $h_2=3$ mm, $h_3=0.5$ mm (c) $V_g=10$ t, $h_2=2$ mm, $h_3=1$ mm, $V_g=10$ t

beam has been modelled and analyzed. It has been assumed that the beam is under electrostatic actuation due to the emitting electrons by a radioisotope electrode layer at the opposite side of the beam. When the electrostatic force overcomes to the bending resistance of system, the beam moves toward the electrode layer, and strikes to the radioisotope material. After discharging the beam is released and oscillation of the beam is started. The piezoelectric layer converts the released microbeam vibration into electricity. The equation of motion has been obtained using Hamilton's principle. The differential equation governed on the piezoelectric output voltage coupled to the motion equation of the beam has been obtained employing Gauss's law. The system equations has been discretized by Galerkin method, and then solved using Runge-Kutta numerical method. The effect of cavity thickness and its position on the output electrical voltage have been investigated.

The results demonstrated that the maximum output voltage and electrical power may be increased by creating a cavity along the length of the beam. The results indicated that the maximum output

voltage and electrical power increases to a special value and then decreases by increasing the cavity thickness. In other words, there is an optimal thickness for cavity to generate the maximum output power. The results also showed that the maximum output voltage and electrical power decreases by increasing the cavity distance from the upper surface of the beam. The effect of the electrical resistance of piezoelectric layer on the output electrical power was also investigated. It has been shown that the maximum electrical output power increases and then decreases by an increase of the electrical resistance of the piezoelectric layer. The result showed that the rate of emitting electrode by radioisotopes layer had no effect on the maximum output power; but it has a significant effect on the total harvested electrical power during a period of time.

References

- Abdelkefi, A., Najar, F., Nayfeh, A.H. and Ayed, S.B. (2011), "An energy harvester using piezoelectric cantilever beams undergoing coupled bending–torsion vibrations", *Smart Mater. Struct.*, **20**(11), 115007.
- Abdelkefi, A., Nayfeh, A.H. and Hajj, M.R. (2012), "Modeling and analysis of piezoaeroelastic energy harvesters", *Nonlin. Dyn.*, **67**(2), 925-939. <https://doi.org/10.1007/s11071-011-0035-1>.
- Amini, Y., Heshmati, M., Fatehi, P. and Habibi, S.E. (2017), "Piezoelectric energy harvesting from vibrations of a beam subjected to multi-moving loads", *Appl. Math. Model.*, **49**, 1-16. <https://doi.org/10.1016/j.apm.2017.04.043>.
- Beer, F.P., Johnston Jr, E.R., Dewolf, J.T. and Mazurek, D.F. (2010), *Mechanics of Materials*, Sixth Edit Edition.
- Brufau-Penella, J. and Puig-Vidal, M. (2009), "Piezoelectric energy harvesting improvement with complex conjugate impedance matching", *J. Intel. Mater. Syst. Struct.*, **20**(5), 597-608. <https://doi.org/10.1177/1045389X08096051>.
- Chen, X.R., Yang, T.Q., Wang, W. and Yao, X. (2012), "Vibration energy harvesting with a clamped piezoelectric circular diaphragm", *Ceram. Int.*, **38**, S271-S274. <https://doi.org/10.1016/j.ceramint.2011.04.099>.
- Deepesh, U., Li, X. and Yang, Y. (2020), "Analytical and experimental investigation of stepped piezoelectric energy harvester", *Smart Struct. Syst.*, **26**(6), 681-692. <https://doi.org/10.12989/sss.2020.26.6.681>.
- Dow, A.B.A., Schmid, U. and Kherani, N.P. (2011), "Analysis and modeling of a piezoelectric energy harvester stimulated by β -emitting radioisotopes", *Smart Mater. Struct.*, **20**(11), 115019.
- Dutoit, N.E., Wardle, B.L. and Kim, S.G. (2005), "Design considerations for MEMS-scale piezoelectric mechanical vibration energy harvesters", *Integ. Ferroelec.*, **71**, (1), 121-160. <https://doi.org/10.1080/10584580590964574>.
- Erturk, A. and Inman, D.J. (2008), "Issues in mathematical modeling of piezoelectric energy harvesters", *Smart Mater. Struct.*, **17**(6), 065016.
- Erturk, A. and Inman, D.J. (2009), "An experimentally validated bimorph cantilever model for piezoelectric energy harvesting from base excitations", *Smart Mater. Struct.*, **18**(1), 025009.
- Firouzi, B. and Zamanian, M. (2019), "The effect of capillary and intermolecular forces on instability of the electrostatically actuated microbeam with T-shaped paddle in the presence of fringing field", *Appl. Math. Model.*, **71**, 243-268. <https://doi.org/10.1016/j.apm.2019.02.016>.
- Franco, V.R. and Varoto, P.S. (2017), "Parameter uncertainties in the design and optimization of cantilever piezoelectric energy harvesters", *Mech. Syst. Signal Pr.*, **93**, 593-609. <https://doi.org/10.1016/j.ymsp.2017.02.030>.
- Ghodsii, M., Ziaiefar, H., Mohammadzaheri, M., Omar, F. K. and Bahadur, I. (2019), "Dynamic analysis and performance optimization of permendur cantilevered energy harvester", *Smart Struct. Syst.*, **23**(5), 421-428. <http://doi.org/10.12989/sss.2019.23.5.421>.
- Guan, Q.C., Ju, B., Xu, J.W., Liu, Y.B. and Feng, Z.H. (2013), "Improved strain distribution of cantilever

- piezoelectric energy harvesting devices using H-shaped proof masses”, *J. Intel. Mater. Syst. Struct.*, **24**(9), 1059-1066. <https://doi.org/10.1177/1045389X13476150>.
- Junior, C.D.M., Erturk, A. and Inman, D.J. (2009), “An electromechanical finite element model for piezoelectric energy harvester plates”, *J. Sound Vib.*, **327**(2), 9-25. <https://doi.org/10.1016/j.jsv.2009.05.015>.
- Kim, C., Ko, Y., Kim, T., Yoo, C. S., Choi, B., Han, S. H., ... & Kim, N. (2018), “Design and evaluation of an experimental system for monitoring the mechanical response of piezoelectric energy harvesters”, *Smart Struct. Syst.*, **22**(2), 133-137. <https://doi.org/10.12989/sss.2018.22.2.133>.
- Kim, N. L., Jeong, S.S., Cheon, S.K., Park, T.G. and Kim, M.H. (2013), “Generating characteristics of hollow-plate-type piezoelectric energy harvesters”, *J. Korean Phys. Soc.*, **63**(12), 2310-2313. <https://doi.org/10.3938/jkps.63.2310>.
- Li, W.G., He, S. and Yu, S. (2009), “Improving power density of a cantilever piezoelectric power harvester through a curved L-shaped proof mass”, *IEEE Tran. Indus. Elec.*, **57**(3), 868-876. <https://doi.org/10.1109/TIE.2009.2030761>.
- Mehraeen, S., Jagannathan, S. and Corzine, K.A. (2009), “Energy harvesting from vibration with alternate scavenging circuitry and tapered cantilever beam”, *IEEE Tran. Indus. Elec.*, **57**(3), 820-830. <https://doi.org/10.1109/TIE.2009.2037652>.
- Mishra, K., Panda, S.K., Kumar, V. and Dewangan, H.C. (2020), “Analytical evaluation and experimental validation of energy harvesting using low-frequency band of piezoelectric bimorph actuator”, *Smart Struct. Syst.*, **26**(3), 391-401. <https://doi.org/10.12989/sss.2020.26.3.391>.
- Muralt, P. (2000), “Ferroelectric thin films for micro-sensors and actuators: A review”, *J. Micromech. Microeng.*, **10**(2), 136.
- Priya, S. (2007), “Advances in energy harvesting using low profile piezoelectric transducers”, *J. Electroceram.*, **19**(1), 167-184. <https://doi.org/10.1007/s10832-007-9043-4>.
- Pan, D. and Dai, F. (2018), “Design and analysis of a broadband vibratory energy harvester using bi-stable piezoelectric composite laminate”, *Energy Convers. Manage.*, **169**, 149-160. <https://doi.org/10.1016/j.enconman.2018.05.032>.
- Rami Reddy, A., Umopathy, M., Ezhilarasi, D. and Gandhi, U. (2016), “Improved energy harvesting from vibration by introducing cavity in a cantilever beam”, *J. Vib. Control*, **22**(13), 3057-3066. <https://doi.org/10.1177/1077546314558498>.
- Rao, S.S. (2007), *Vibration of Continuous Systems*, Vol. 464, Wiley, New York.
- Roundy, S. and Wright, P.K. (2004), “A piezoelectric vibration based generator for wireless electronics”, *Smart Mater. Struct.*, **13**(5), 1131.
- Sarker, M.R., Julai, S., Sabri, M.F.M., Said, S.M., Islam, M.M. and Tahir, M. (2019), “Review of piezoelectric energy harvesting system and application of optimization techniques to enhance the performance of the harvesting system”, *Sensor. Actuat. A: Phys.*, **300**, 111634. <https://doi.org/10.1016/j.sna.2019.111634>.
- Sodano, H.A., Inman, D.J. and Park, G. (2004), “A review of power harvesting from vibration using piezoelectric materials”, *Shock Vib. Digest*, **36**(3), 197-206.
- Usharani, R., Uma, G., Umopathy, M. and Choi, S.B. (2017), “A new broadband energy harvester using propped cantilever beam with variable overhang”, *Smart Struct. Syst.*, **19**(5), 567-576. <http://doi.org/10.12989/sss.2017.19.5.567>.
- Wang, J., Zhao, G. and Zhang, H. (2009), “Optimal placement of piezoelectric curve beams in structural shape control”, *Smart Struct. Syst.*, **5**(3), 241-260. <http://doi.org/10.12989/sss.2009.5.3.241t>.
- Wang, Z. and Xu, Y. (2007), “Vibration energy harvesting device based on air-spaced piezoelectric cantilevers”, *Appl. Phys. Lett.*, **90**(26), 263512. <https://doi.org/10.1063/1.2752726>.
- Zamanian, M., Javadi, S., Firouzi, B. and Hosseini, S.A.A. (2018), “Modeling and analysis of power harvesting by a piezoelectric layer coated on an electrostatically actuated microcantilever”, *Mater. Res. Express*, **5**(12), 125502.
- Zamanian, M., Rezaei, H., Hadilu, M. and Hosseini, S.A.A. (2015), “A comprehensive analysis on the discretization method of the equation of motion in piezoelectrically actuated microbeam”, *Smart Struct. Syst.*, **16**(5), 891-918. <http://doi.org/10.12989/sss.2015.16.5.891>.

- Zhang, Y. and Zhu, B. (2012), "Analysis and simulation of multi-mode piezoelectric energy harvesters", *Smart Struct. Syst.*, **9**(6), 549-563. <http://doi.org/10.12989/sss.2012.9.6.549>.
- Zhao, D., Gan, M., Zhang, C., Wei, J., Liu, S. and Wang, T. (2018), "Analysis of broadband characteristics of two degree of freedom bistable piezoelectric energy harvester", *Mater. Res. Express*, **5**(8), 085704.

Appendix A

Expressions including damping and voltage in Eq. (23) are excluded; therefore the free vibration equation of system will be as below

$$m(x) \frac{\partial^2 v}{\partial \tau^2} + \frac{\partial^2}{\partial x^2} \left(H(x) \frac{\partial^2 v}{\partial x^2} \right) = 0 \quad (\text{A.1})$$

The free vibration response of system is assumed as below

$$v(x, \tau) = \varphi_i(x) e^{i\omega\tau} \quad (\text{A.2})$$

Where $\varphi(x)$ is the mode shape of system, and ω is the natural frequency. By substituting Eq. (A-2) into Eq. (A-1) one obtains

$$-\omega^2 m(x) \varphi(x) + \frac{d^2}{dx^2} \left(H(x) \frac{d^2 \varphi}{dx^2} \right) = 0 \quad (\text{A.3})$$

To solve the above equation, the system is divided into three parts as

$$\begin{cases} -\omega^2 \varphi(x) + \frac{d^4 \varphi(x)}{dx^4} = 0, & 0 \leq x < \frac{l_1}{l}, \\ -\left(1 + \frac{\rho_p \hat{h}_p - \rho_b \hat{h}_b}{\rho_b \hat{h}_b} \right) \omega^2 \varphi(x) + \left(\frac{I_{2b}}{I_{1b}} + \frac{I_{3b}}{I_{1b}} + \frac{E_p I_p}{E_b I_b} \right) \frac{d^4 \varphi(x)}{dx^4} = 0, & \frac{l_1}{l} < x < \frac{l_2}{l}, \\ -\omega^2 \varphi(x) + \frac{d^4 \varphi(x)}{dx^4} = 0 & \frac{l_2}{l} < x \leq 1 \end{cases} \quad (\text{A.4})$$

By solving the above equation, $\varphi(x)$ is obtained in three parts as follows

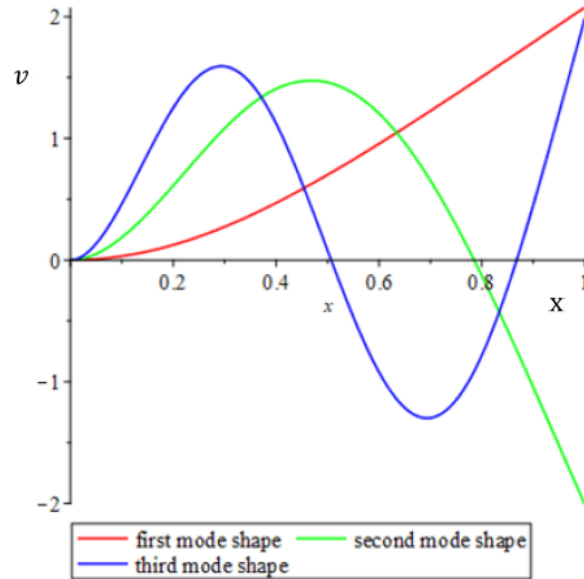
$$\begin{cases} \varphi(x) = C_1 \cosh(\beta_1 x) + C_2 \sinh(\beta_1 x) + C_3 \cos(\beta_1 x) + C_4 \sin(\beta_1 x), & 0 \leq x < \frac{l_1}{l}, \\ \varphi(x) = C_5 \cosh(\beta_2 x) + C_6 \sinh(\beta_2 x) + C_7 \cos(\beta_2 x) + C_8 \sin(\beta_2 x), & \frac{l_1}{l} < x < \frac{l_2}{l}, \\ \varphi(x) = C_9 \cosh(\beta_1 x) + C_{10} \sinh(\beta_1 x) + C_{11} \cos(\beta_1 x) + C_{12} \sin(\beta_1 x), & \frac{l_2}{l} < x \leq 1 \end{cases} \quad (\text{A.5})$$

where C_i are constant coefficients that are calculated from boundary and continuity conditions due to equality the amount of shear force and moment at the stepped cross section, i.e.

$$\begin{aligned} \varphi|_{x=0} = 0, \quad \frac{d\varphi}{dx}|_{x=0} = 0, \quad \frac{d^2 \varphi}{dx^2}|_{x=1} = 0, \quad \frac{d^3 \varphi}{dx^3}|_{x=1} = 0 \\ \varphi|x = l_1/l = \varphi|x = l_1/l, \quad \frac{d\varphi}{dx}|x = l_1/l = \frac{d\varphi}{dx}|x = l_1/l, \\ \frac{d^2 \varphi}{dx^2}|x = l_1/l = \left(\frac{I_{2b}}{I_{1b}} + \frac{I_{3b}}{I_{1b}} + \frac{E_p I_p}{E_b I_b} \right) \frac{d^2 \varphi}{dx^2}|x = l_1/l, \\ \frac{d^3 \varphi}{dx^3}|x = l_1/l = \left(\frac{I_{2b}}{I_{1b}} + \frac{I_{3b}}{I_{1b}} + \frac{E_p I_p}{E_b I_b} \right) \frac{d^3 \varphi}{dx^3}|x = l_1/l, \end{aligned}$$

$$\beta_1 = \sqrt{\omega}, \quad \beta_2 = \left(\frac{\left(1 + \frac{\rho_p h_p - \rho_b h_2}{\rho_b h_b} \right)}{\left(\frac{I_{2b} + I_{3b} + \frac{E_p I_p}{E_b I_b} \right)} \omega^2 \right)^{\frac{1}{4}} \quad (\text{A.6})$$

Three mode shapes of system calculated according to the above approach have been shown in the following figure.



Three mode shapes of system where $h_2=2$ mm and $h_3=0.5$ mm